

Artificial Solid-Electrolyte Interphase with PVDF-ZnF₂ Double-Layer Structures Enhancing Electrochemical Performance of Sodium Metal Batteries

Kaichen Yu,^[a] Jinbiao Chen,^[a, b] Zhifeng Xiao,^[a] Yuqing Yang,^[c] Yanpeng Fu,^[a] Abdullah N. Alodhayb,^[d] Jie Li,^{*[b]} Chunsheng Li,^{*[c]} Yan Sun,^[c] and Zhicong Shi^{*[a, e]}

Sodium metal batteries (SMBs) have attracted significant attention due to their high theoretical capacity and abundant resources. However, commercialization for this cell is challenged by the high reactivity of sodium metal, leading to detrimental side reactions with electrolytes, dendritic growth, and severe volume changes over charging/discharging cycles. These issues shorten the cycle life, reduce efficiency, and increase the risk of internal short circuits and thermal runaway. A stable solid electrolyte interphase (SEI) is key to addressing these challenges by preventing dendrite growth, homogenizing sodium ion transport, and maintaining chemical stability. This study inves-

tigates an artificial SEI(ASEI) composed of polyvinylidene fluoride (PVDF) and ZnF₂, which forms a durable organic-inorganic double-layer structure. The outer organic PVDF layer enhances mechanical strength, while the inner inorganic ZnF₂ layer improves sodium ion flux, preventing dendritic growth. The ASEI significantly extends cell life and enhance electrochemical performances. The NVP|50 μL –4 wt.% + 100 μL –8 wt.% PVDF-ZnF₂/Na cell demonstrates stable cycling for over 3000 cycles. This novel ASEI design offers promising potential for improving the energy storage properties and safety of sodium metal batteries.

Introduction

Sodium metal batteries have become a research hotspot in the field of energy storage because of their super higher theoretical capacity than that of sodium ionic batteries.^[1,2] Sodium metal anode has a high specific capacity and low redox potential,^[3,4] showing an ideal anode material for constructing high specific-energy sodium-based batteries.^[5–7] Sodium element has obvious advantages in large-scale applications for abundant resources and low price.^[8–11] However, commercializing sodium metal batteries still faces certain challenges. The high chemical reactivity of sodium metal will lead to irreversible side reactions with organic electrolytes and the growth of large amounts of

sodium dendrites will result in large volume change, low actual volume capacity, and short cycle life.^[12–14] The cracks on solid electrolyte interphase (SEI), caused by the enlarged volume change during initial cycles, will permit the infiltration of electrolyte to react with the following Na metal anode, and further promote the growth of sodium dendrites.^[15,16] On the other hand, sodium dendrites will form “dead sodium” in the process of sodium metal stripping, attributing to the huge layered volume.^[17] The continuous vicious cycle leads to internal short circuits and thermal runaway in sodium metal batteries, and even combustion and explosion.^[17,18]

It has been proved that the construction of stable SEI can effectively inhibit the growth of dendrites and reduce volume expansion.^[15,19,20] The ideal SEI has the following characteristics: (1) mechanical stability to prevent SEI from cracking;^[21] (2) uniform Na⁺ transport channels to homogenize sodium metal deposition;^[22] (3) chemical stability to prevent the Na metal anode from reacting with the liquid electrolyte.^[23] In recent years, it has attracted researchers’ attention to design the composition and structure of SEI of sodium metal anode by ex-situ method, which can homogenize the sodium ion flux and inhibit the growth of sodium dendrites, to maintain the stability of sodium metal.^[24–26]

Among designs of ASEI, inorganic ASEI has an excellent ion conduction performance among sorts of designs for ASEI, which can greatly improve the distribution of sodium ions on the surface of sodium metal anode, homogenize the transport of sodium ions, and inhibit the growth of dendrites.^[27,28] Components, such as Bi,^[29] SbF₃,^[30] SnS,^[31] or BiOCl,^[32] Al₂O₃,^[33] red phosphorus (P),^[14] will form sodium compounds and alloys during the cell cycle. The inorganic phase has higher ion conductivity, accelerates charge transfer kinetics, reduces

[a] K. Yu, J. Chen, Z. Xiao, Y. Fu, Z. Shi
Institute of Batteries, School of Materials and Energy, Guangdong University of Technology, Guangzhou 510006, China
E-mail: zhicong@gdut.edu.cn

[b] J. Chen, J. Li
Department of Energy, Politecnico di Milano, Via Lambruschini, 4, Milan 20156, Italy
E-mail: jie1.li@polimi.it

[c] Y. Yang, C. Li, Y. Sun
Key Laboratory of Advanced Electrode Materials for Novel Solar Cells for Petroleum and Chemical Industry of China, School of Chemistry and Life Sciences, Suzhou University of Science and Technology, Suzhou City, Jiangsu Province 215009, China
E-mail: lichsheng@163.com

[d] A. N. Alodhayb
Department of Physics and Astronomy, College of Science, King Saud University, Riyadh 11451, Saudi Arabia

[e] Z. Shi
Key Laboratory of Advanced Energy Materials Chemistry (Ministry of Education), Nankai University, Tianjin 300071, China

charge transfer, reduces the non-uniform distribution of sodium ions on the surface of sodium metal, and inhibits dendrite growth.^[34–36] However, the symmetric cells show a continuous increase of overvoltage during cycling.^[37] Although the alloy layer can effectively inhibit the formation of dendrites, the performance of SMB is still affected by the imperfect SEI film.^[38] For example, the mechanical strength of inorganic ASEI is still low, and inorganic ASEI is susceptible to irreversible damage due to volume expansion during the metal negative cycle.^[26] Many alloy components are electrically conductive, and alloying groups induce sodium metal deposition at the interface between the electrolyte and SEI.^[39]

Besides, polymers with specific mechanical strength and stability,^[35] such as poly (vinylidene fluoride) (PVDF)^[40] and PE^[41] have been also successfully used to prepare the ASEI on the Na anode. The polymer PVDF is commonly used as a binder in commercial Li-ion batteries due to its good elastic property, stability, and ion transport ability.^[41] Nonetheless, the PVDF binder suffers from a low mechanical modulus and ion diffusion conductivity,^[14] which cannot satisfy the requirements of an ideal SEI in SMBs.

The construction of organic and inorganic composite double-layer ASEI can combine the advantages of the two and make up for defects of each other.^[27,42] The organic surface layer has high mechanical strength and the ASEI is not easy to be damaged. The inorganic inner layer can serve as a buffer layer for uniform sodium ion transport and homogenize the deposition of sodium metal. Building a stable two-layer ASEI can greatly improve the physical and chemical properties of SEI.

The chemical reaction on the surface of sodium metal is strongly uncontrollable due to the high activity of sodium metal, and the thickness and structure of ASEI constructed cannot be accurately controlled.^[26,43,44] A stable ASEI is constructed prior to battery assembly. In the process of battery assembly, the ASEI is pressed to make close contact with sodium metal. In the formation stage, the ASEI reacts with the surface of sodium metal to form a double-layer ASEI in close contact with sodium metal. This method can effectively construct a stable double-layer structure and precisely control the thickness of the organic and inorganic layers.

Experimental Section

Preparation of PVDF-ZnF₂–Na Anode

A 4 wt.% PVDF/NMP solution was prepared using a magnetic stirrer at 80 °C for 4 hours to ensure uniformity. The resulting solution was then poured onto a 15 mm diameter glass sheet in volumes of 50, 100, and 150 μL, respectively. The samples were placed in a vacuum drying oven at 120 °C for 12 hours. After the complete evaporation of the NMP solvent, a homogeneous PVDF layer was obtained on the glass sheet.

4 wt.% and 8 wt.% ZnF₂/NMP suspension were prepared after 4 hours ultrasonic processing. PVDF powder was added to the ZnF₂/NMP suspension at a mass ratio of ZnF₂: PVDF = 9:1 and stirred at 80 °C for 4 hours to obtain a homogeneous PVDF-ZnF₂/NMP. 50 μL and 100 μL of the PVDF-ZnF₂/NMP mixture were poured

on a glass sheet pre-coated with different volumes of PVDF, respectively. The glass substrate was then placed in a vacuum drying oven and dried at 120 °C for 10 min to completely evaporate the NMP. After drying, the film was removed from the surface of the glass substrate to obtain PVDF-ZnF₂ composite film samples with different proportions. The film of different ratios is pressed onto the polished sodium sheet to obtain different PVDF-ZnF₂–Na anodes (Fig. 1a). The films of different ratios are named A μL –B wt.% + C μL –D wt.% PVDF-ZnF₂, where A and B are respectively the volume and mass ratio of PVDF/NMP, respectively. C and D are the volume and mass ratio of ZnF₂/NMP, respectively. For example, the “50 μL –4 wt.% + 100 μL –8 wt.%” refers to a PVDF-ZnF₂ composed of 50 μL of 4 wt.% PVDF/NMP and 100 μL of 8 wt.% ZnF₂/NMP.

Characterizations

Morphology of pristine and cycled electrodes was observed by scanning electron microscopy (SEM, Hitachi), which was operated at an accelerating voltage of 5–10 kV. Before the SEM measurement, the cycled electrodes were immersed and washed with 1,2-Dimethoxyethane (DME) for three times to remove the surficial residues. After immersing in liquid nitrogen for 10 minutes, the samples were carefully folded in half using insulated tweezers in the liquid nitrogen to obtain cross-sectional surfaces that were then observed using SEM. X-ray diffraction (XRD, D8 ADVANCE) using a Cu Kα radiation source at a wavelength of 0.1514 nm was used to characterize the structure of samples. X-ray photoelectron spectroscopy (XPS, Escalab 250Xi) spectra were recorded by using a monochromatic Al Kα X-ray source.

Electrochemical Measurements

The Na metal anodes were tested in CR-2032 coin cells, which were assembled in an argon-filled glove box with an oxygen and water level below 0.1 ppm. For symmetric cells, 1 M NaPF₆ in Ethylene carbonate (EC)/Diethyl carbonate (DEC) (1:1 in vol/vol) with 5 wt.% Fluoroethylene carbonate (FEC) (DODOCHEM) was applied as electrolyte and glass fiber as the separator. For the full cell measurements, Na₃V₂(PO₄)₃ (NVP) (Canrd, China) was used as the cathode material. The cathode electrode was prepared by casting a slurry of 80 wt.% NVP, 10 wt.% super P (Canrd, China), and 10 wt.% PVDF (Canrd, China) in NMP onto carbon-coated aluminum foil. After drying at 80 °C under vacuum for 12 h, the cathode was punched into a disk with a diameter of 10 mm with the mass loading of NVP on each electrode of 3 mg/cm². 1 M NaPF₆ in EC/DEC (V:V=1:1) with 5 wt.% FEC and glass fibers were used as electrolyte and separator. The full cells were tested at 2 C (1 C = 117.3 mAh g⁻¹) between 2.2 and 3.8 V, respectively. The cells were performed on a LAND electrochemical testing system. Electrochemical impedance spectroscopy (EIS) tests were performed on a SOLARTRON SI1260 applying an alternating voltage of 5 mV over the frequency range from 100 kHz to 10 mHz.

Results and Discussion

XRD and XPS were applied for phase and elemental analyses of the 50 μL - 4 wt.% + 100 μL - 8 wt.% PVDF-ZnF₂ film respectively. All reflections in the XRD pattern are assigned to ZnF₂ (PDF#07-0214) (Figure 1b). Elemental analysis of the 50 μL - 4 wt.% + 100 μL - 8 wt.% PVDF-ZnF₂ films via XPS revealed the presence of carbon (C), fluorine (F), and zinc (Zn). The high-resolution XPS spectrum of C displays peaks of 284.8, 286.1,

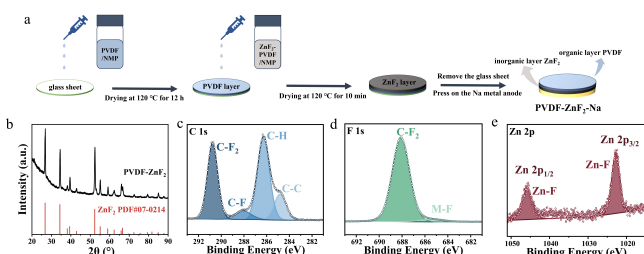


Figure 1. (a) Schematic illustration of the experimental procedure for structuring PVDF-ZnF₂-Na anode. (b) XRD pattern of PVDF-ZnF₂ film, XPS spectra of (c) C 1s, (d) F 1s and (e) Zn 2p of PVDF-ZnF₂-Na anode.

288.0, and 290.9 eV, corresponding to C–C, C–H, C–F, and C–F₂ bonds in PVDF, respectively (Figure 1c).^[45] The high-resolution spectrum of F, the peaks are attributed to C–F₂ in PVDF^[45] and MF (M for metal) in ZnF₂.^[46] (Figure 1d). The spectrum of Zn shows satellite peaks at 1022.8 eV and 1045.8 eV for Zn 2p_{3/2} and Zn 2p_{1/2} of Zn–F, respectively (Figure 1e).^[47] Therefore, it can be accurately concluded that the ASEI is composed of organic PVDF and inorganic ZnF₂.

SEM and EDS was used to observe the surface morphology and cross-sectional thickness of PVDF-ZnF₂ films with different proportions. The surface of organic layer of all proportion of PVDF-ZnF₂ films are distributed by C and F elements, and smooth and free of holes (Figure 2a). The difference of element distribution between surfaces of organic layer and inorganic layer indicates a double-layer structure of the composite films. However, the distribution of the inorganic ZnF₂ layer varies with different mass ratios. ZnF₂ is unevenly distributed, leaving significant exposure of PVDF on the surface of inorganic layer of 4 wt.% PVDF-ZnF₂ film (Figure 2b). In contrast, the surface of inorganic layer of 8 wt.% PVDF-ZnF₂ film exhibits a more

uniform coverage of ZnF₂ particles, with no noticeable unevenness due to particle accumulation (Figure 2c).

The cross sections of the PVDF-ZnF₂ films, observed after brittle fracture in liquid nitrogen, revealed an organic-inorganic double-layer structure. Different volumes of PVDF/NMP solution result in varying thicknesses of the organic layer. Total thicknesses of 50 μL –4 wt.% + 100 μL –4 wt.%, 50 μL –4 wt.% + 100 μL –8 wt.%, 100 μL –4 wt.% + 100 μL –4 wt.%, 100 μL –4 wt.% + 100 μL –8 wt.%, 150 μL –4 wt.% + 100 μL –8 wt.% PVDF-ZnF₂ films are 7.5 (Figure 3a), 25.3 (Figure 3b), 14.1 (Figure 3c), 30.7 (Figure 3d), 17.6 (Figure 3e), and 35.6 μm (Figure 3f), respectively. Specifically, casting 50, 100, and 150 μL of PVDF/NMP solution can produce organic layers with thicknesses of about 1.9, 7.9, and 12.4 μm, respectively (Figure 3a, c, and e). Additionally, the density of the inorganic layer varies significantly depending on the mass ratio of ZnF₂ in PVDF-ZnF₂/NMP. When using a 4 wt.% PVDF-ZnF₂/NMP suspension, the ZnF₂ particles in the as-prepared film are not densely distributed and fully encapsulated by PVDF with a thickness of 5 μm (Figure 3a, c, and e). In contrast, 8 wt.% PVDF-ZnF₂/NMP suspension results in a densely packed ZnF₂ layer in the as-prepared film with a thickness of 22 μm (Figure 3b, d, and f), clearly exhibiting a double-layer structure with the outside organic PVDF layer and the inside ZnF₂ inorganic layer contacting Na anode. The cross-sectional images confirm that the experimental process successfully produced these PVDF-ZnF₂ films, with the thickness of both the organic and inorganic layers varying depending on the casting suspension volume used. It is feasible to control the thickness of the ASEI by adjusting the volume of the casting suspension.

The effect of ASEI thickness on the performances of sodium metal batteries were characterized by assembling the varying thicknesses of ASEI into symmetrical cells. As shown in Figure 4, the symmetric cells with different PVDF-ZnF₂ films demonstrate distinct cycle stability and voltage variation trends at a constant current density of 0.5 mA cm⁻² and a capacity limit of 0.5 mAh cm⁻². There is a rule that the overpotential of symmetric cells increases with the organic layer thickness. The overpotentials of symmetric cells with the same ZnF₂ content of 100 μL –8 wt.% are 120 mV, 170 mV, and 220 mV corresponding to the PVDF content of 50 μL –4 wt.%, 100 μL –4 wt.%, and 150 μL

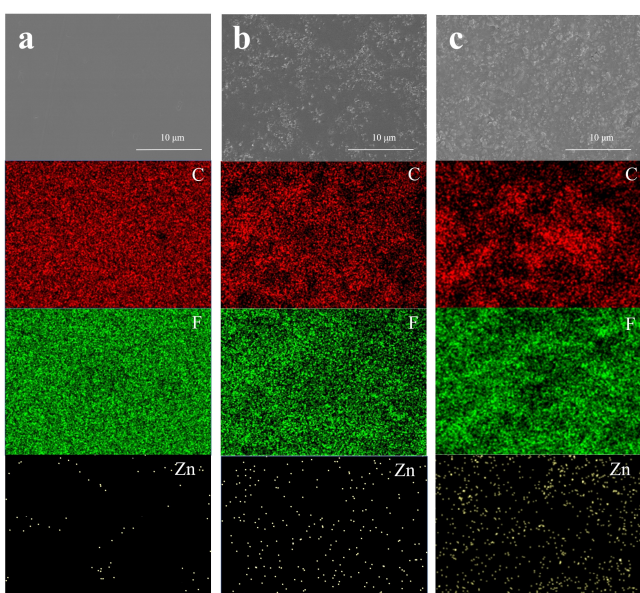


Figure 2. Top-view SEM images with C, F and Zn elements mapping platinum of (a) the organic surface of PVDF-ZnF₂, (b) the inorganic surface of 4 wt.% ZnF₂/NMP, and (c) the inorganic surface of 8 wt.% ZnF₂/NMP.

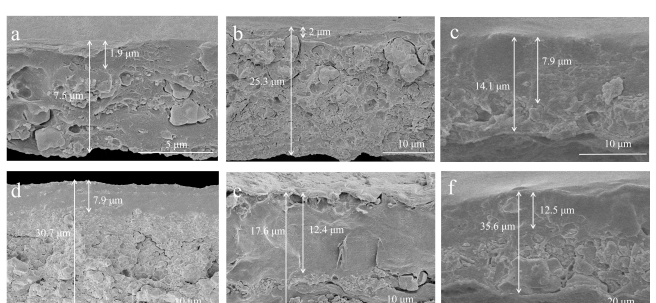


Figure 3. The cross-sectional SEM images of (a) 50 μL –4 wt.% + 100 μL –4 wt.%, (b) 50 μL –4 wt.% + 100 μL –8 wt.%, (c) 100 μL –4 wt.% + 100 μL –4 wt.%, (d) 100 μL –4 wt.% + 100 μL –8 wt.%, (e) 150 μL –4 wt.% + 100 μL –4 wt.%, and (f) 150 μL –4 wt.% + 100 μL –8 wt.% PVDF-ZnF₂ films.

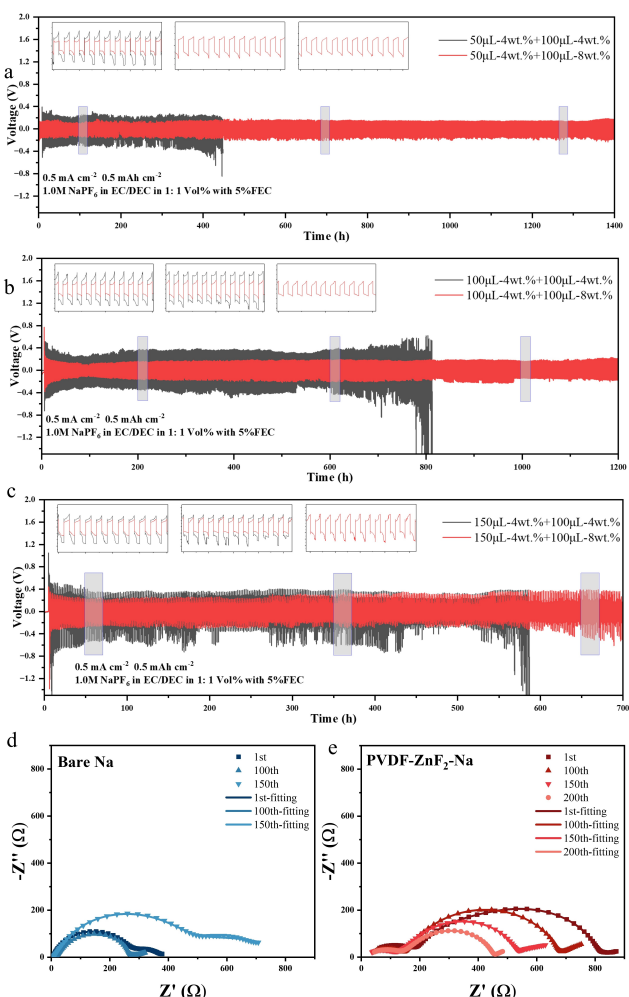


Figure 4. Voltage-time profiles of symmetric cells assembled with (a) 50 μL –4 wt.% + 100 μL –4 wt.% and 50 μL –4 wt.% + 100 μL –8 wt.% PVDF-ZnF₂–Na, (b) 100 μL –4 wt.% + 100 μL –4 wt.% and 100 μL –4 wt.% + 100 μL –8 wt.% PVDF-ZnF₂–Na, and (c) 150 μL –4 wt.% + 100 μL –4 wt.% and 150 μL –4 wt.% + 100 μL –8 wt.% PVDF-ZnF₂–Na at current densities of 0.5 mA cm^{-2} for 1 h. Nyquist plots of symmetric cells with (d) bare Na and (e) 50 μL –4 wt.% + 100 μL –8 wt.% PVDF-ZnF₂–Na during repeated cycles.

–4 wt.%, increasing as the organic layer thickness, respectively. The symmetrical cell with the 50 μL –4 wt.% + 100 μL –4 wt.% PVDF-ZnF₂ film has a dramatic decline in overpotential after 450 hours, (Figure 4a). On the other hand, the symmetrical cell built with the 50 μL –4 wt.% + 100 μL –8 wt.% PVDF-ZnF₂ film shows a longer stable cycle life by sustaining a steady overpotential for 1400 hours. While the cell with the 100 μL –4 wt.% + 100 μL –8 wt.% PVDF-ZnF₂ film has a longer stable cycle life of 1200 hours, the symmetrical cell with the 100 μL –4 wt.% + 100 μL –4 wt.% PVDF-ZnF₂ film shows a voltage rise to 1.0 V after 800 hours (Figure 4b). The symmetrical cell with the 150 μL –4 wt.% + 100 μL –4 wt.% PVDF-ZnF₂ film exhibits cycle stability for 700 hours, but the cell with the 150 μL –4 wt.% + 100 μL –8 wt.% PVDF-ZnF₂ film has an overpotential surge to 1.0 V at 580 hours (Figure 4c). It is concluded that symmetric cells can sustain a lower overpotential and stable cycling for a longer amount of time due to a thinner organic

layer and a homogeneous inorganic layer. On the contrary, bared Na demonstrates stable cycling with a minor overpotential for roughly 380 h before encountering a sudden voltage drop. In conclusion, the non-uniformity of the inorganic layer leads to an increasing overpotential of the symmetric cell, and the uneven deposition of sodium metal results in short circuits, ultimately reducing the cycle life of the sodium metal anode.

Additionally, electrochemical impedance spectroscopy (EIS) experiments were conducted to investigate the interface characteristics of the symmetric cells in SMBs. The interfacial impedance (R_{SEI}) of the bare Na decreases from 52.77 Ω in the initial cycle to 20.27 Ω after 100 cycles, but sharply increases to 371.8 Ω after the 150th cycle (Figure 4d), possibly originated to the destruction and subsequent reconstruction of the SEI layer as well as the formation of “dead Na”. In contrast, the R_{SEI} of PVDF-ZnF₂–Na continuously decreases from 200 Ω in the first cycle to 171 Ω after the 200th cycle (Figure 4e). Symmetric cells with PVDF-ZnF₂–Na demonstrate stable interface impedance throughout repeated cycling, indicating that the PVDF-ZnF₂–Na anode maintains a consistent electrochemical interface. The PVDF-ZnF₂–Na anode, compared with bare Na, exhibits superior characteristics in terms of dendrite growth inhibition and maintaining interfacial stability during the Na deposition/stripping process.

The symmetrical cell with the 50 μL –4 wt.% + 100 μL –8 wt.% PVDF-ZnF₂ film is cycled for 50 cycles at a current density of 0.5 mA cm^{-2} and a capacity limit of 0.5 mAh cm^{-2} . After cycling, the cell is disassembled, and the surface morphology and cross-section of the deposited side of the film and sodium metal are examined by the SEM measurement (Figure 5a). The surface of the organic layer of the ASEI remains flat and dense, while the surface of the inorganic layer transformed from dispersed ZnF₂ particles into a flat and dense alloy layer. There is a smooth, dense sodium metal surface consisting of numerous nanoscale globular particles below the ASEI film (Figure 5b).

The PVDF-ZnF₂ film was disassembled from the symmetrical cell and immersed in liquid nitrogen. After the brittle fracture, the cross-section of the PVDF-ZnF₂ film was observed using SEM. The organic layer remains intact and dense, while the

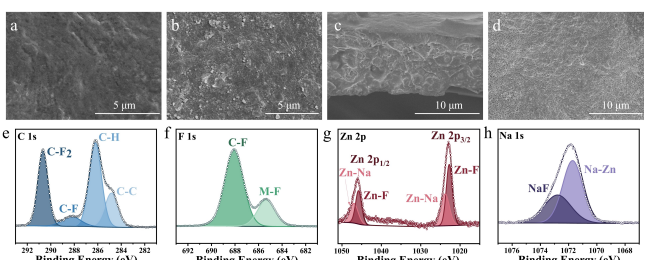


Figure 5. Top-view SEM images of (a) the organic surface and (b) the inorganic surface of cycled 50 μL –4 wt.% + 100 μL –8 wt.% PVDF-ZnF₂–Na. (c) Cross-sectional SEM image of 50 μL –4 wt.% + 100 μL –8 wt.% PVDF-ZnF₂–Na after cycling. (d) Top-view SEM images of the surface of Na metal anode of cycled 50 μL –4 wt.% + 100 μL –8 wt.% PVDF-ZnF₂–Na after cycling. XPS spectra of (e) C 1s, (f) F 1s, (g) Zn 2p and (h) Na 1s of 50 μL –4 wt.% + 100 μL –8 wt.% PVDF-ZnF₂–Na after cycling.

inorganic layer changes from its initial loose and porous state to a dense morphology. The surface and cross-section of the ASEI after cycling indicate that the PVDF-ZnF₂ film retains a distinct double-layer structure and shows no signs of volume expansion after cycling (Figure 5c). Na was uniformly deposited on the surface of sodium metal anode without obvious dendrites growth (Figure 5d). The PVDF layer remains stable due to its mechanical and chemical properties, while the inorganic alloy layer reacts with the deposited sodium metal to form a homogeneous and dense alloy layer, homogenizing sodium ion flux and inhibiting dendrite growth. Consequently, the uniformity and stability of the sodium metal surface are significantly enhanced.

The components of the ASEI after riding are different from the XPS analysis before cycling. Regarding the C element, there are no significant alterations, and the characteristic peaks corresponding to PVDF remained intact. No peaks related to C=O or C–O were detected (Figure 5e). This demonstrates that the PVDF layer maintains its stability throughout the cycling process and effectively prevents the formation of carbonates by shielding the sodium metal from corrosion by organic solvents. However, significant changes were observed in the F and Zn spectra (Figure 5f and g). The M–F and Na–Zn^[48] signals increased notably after cycling. This is since during cycling, the addition of sodium ions causes a reaction between ZnF₂ and Na, resulting in the formation of Na–Zn^[49] and NaF^[50] (Figure 5h). These compounds are superior sodium ion conductors and can effectively reduce dendrite formation by homogenizing the sodium ion flow on the outer surface of the sodium metal anode.

To evaluate the potential practical application of the ASEI in SMBs, full cells were assembled using 50 μL –4 wt.% + 100 μL –8 wt.% and 100 μL - 4 wt.% + 100 μL –8 wt.% PVDF-ZnF₂ films with a Na₃V₂(PO₄)₃ (NVP) cathode. The NVP | 50 μL –4 wt.% + 100 μL –8 wt.% PVDF-ZnF₂/Na cell demonstrates exceptional cycling stability, lasting over 3,000 cycles (Figure 6a). These results highlight that the full cells assembled with the ASEI prepared at a 50 μL –4 wt.% + 100 μL –8 wt.% ratio exhibit significantly better electrochemical performance compared to those with the 100 μL - 4 wt.% + 100 μL –8 wt.% ratio (Figure 6a). The overpotential of NVP | 50 μL –4 wt.% + 100 μL –8 wt.% PVDF-ZnF₂/Na (0.21 V) is slightly higher than that of NVP | bare Na (0.2 V), and the capacity of cell can maintain more than 2000 turns according to the capacity-voltage profiles (Figure 6b). The localized micro short circuits occurring in NVP | bare Na cause excessive charging capacity, leads to large fluctuations in the coulomb efficiency (Figure 6c). Over time, these micro short circuits will cause the short circuit failure and safety problems of the cells. The thickness of the composite film prepared is thicker by the pouring method, which will cause the increase of the overpotential of the cells, and thus affect the capacity of the full cells. And the continuous reaction of the ZnF₂ layer may cause a small capacity loss. However, the composite films can maintain the stability of the sodium metal surface and reduce the growth of dendrites, thus stabilizing the coulomb efficiency and improving the safety of the full cells.

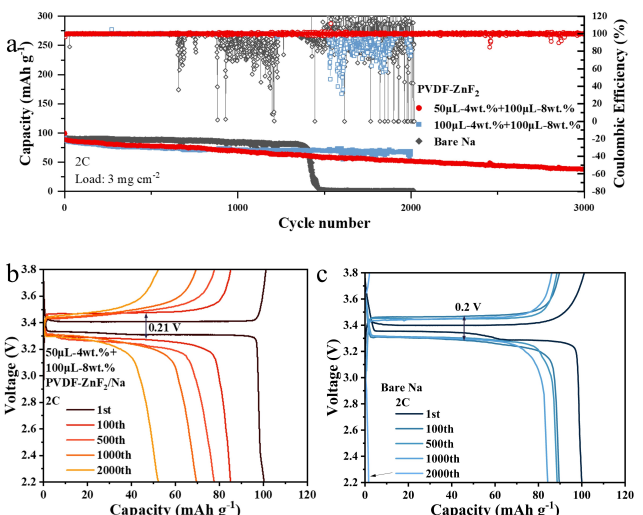


Figure 6. (a) Cycling performance of NVP-based full cells with bare Na, 50 μL –4 wt.% + 100 μL –8 wt.%, and 100 μL - 4 wt.% + 100 μL –8 wt.% PVDF-ZnF₂/Na at 2 C. Discharge-charge profiles with (b) 50 μL –4 wt.% + 100 μL –8 wt.% PVDF-ZnF₂/Na and (c) Bare Na at 2 C.

Thus, the 50 μL –4 wt.% + 100 μL –8 wt.% PVDF-ZnF₂/Na ASEI offers superior electrochemical properties in full-cell applications.

Conclusions

This study successfully addresses the issues of sodium dendrite growth and volume expansion in sodium metal batteries by constructing an organic-inorganic artificial solid electrolyte interphase-made of PVDF and ZnF₂. The experimental results demonstrate that the 50 μL –4 wt.% + 100 μL –8 wt.% ASEI significantly outperforms other ratios in both symmetric and full-cell configurations, especially in terms of cycle life. The dual-layer structure combines the excellent mechanical strength of PVDF with the high ionic conductivity of ZnF₂, facilitating uniform sodium ion deposition and suppressing dendrite formation, thereby enhancing the stability and safety of advanced sodium metal batteries.

Acknowledgements

We gratefully acknowledge the financial support from the Ministry of Science and Technology of People's Republic of China (502220178), the National Natural Science Foundation of China (No. 22379103), the Science and Technology Projects of Suzhou City (SYC2022043), the project of King Saud University, Riyadh, Saudi Arabia (RSP2025R304), and the Qing Lan Project of Jiangsu Province (2022). We wish to thank the Analysis and Test Center, Guangdong University of Technology for the microscopy and microanalysis.

Conflict of Interests

There are no conflicts to declare.

Data Availability Statement

The data that support the findings of this study are available from the corresponding author upon reasonable request.

Keywords: ASEI • Double-layer • Energy storage and conversion • PVDF-ZnF₂ • Sodium metal anode

- [1] Q. Lu, A. Yang, A. Omar, Q. Ma, F. Tietz, O. Guillon, D. Mikhailova, *Energy Technol.* **2022**, *10*(7), 2200149.
[2] C. Zhao, Y. Lu, J. Yue, D. Pan, Y. Qi, Y.-S. Hu, L. Chen, *J. Energy Chem.* **2018**, *27*(6), 1584–1596.
[3] K. Chayambuka, G. Mulder, D. L. Danilov, P. H. Notten, *Adv. Energy Mater.* **2018**, *8*(16), 1800079.
[4] L. Chen, Z. Liu, W. Yang, S. Wu, Y. Li, Y. Zhang, L. Zeng, H. Fan, *J. Colloid Interface Sci.* **2024**, *666*, 416–423.
[5] Z. Bai, Q. Yao, M. Wang, W. Meng, S. Dou, H. K. Liu, N. Wang, *Adv. Energy Mater.* **2024**, *14*(17), 2303788.
[6] M. He, S. Liu, J. Wu, J. Zhu, *Prog. Solid State Chem.* **2024**, 100452.
[7] Y. Zeng, J. Yang, H. Yang, Y. Yang, J. Zhao, *ACS Energy Lett.* **2024**, *9*(3), 1184–1191.
[8] C. Bao, B. Wang, P. Liu, H. Wu, Y. Zhou, D. Wang, H. Liu, S. Dou, *Adv. Funct. Mater.* **2020**, *30*(52), 2004891.
[9] S.-J. Lu, J.-Y. Lin, C.-H. Wang, Y.-F. Zhang, Y. Zhang, H.-S. Fan, *Rare Met.* **2024**, 1–11.
[10] S. Vineeth, C. B. Soni, Y. Sun, V. Kumar, Z. W. She, *Trends Chem.* **2022**, *4*(1), 48–59.
[11] C. Zhao, Q. Wang, Z. Yao, J. Wang, B. Sánchez-Lengeling, F. Ding, X. Qi, Y. Lu, X. Bai, B. Li, *Science* **2020**, *370*(6517), 708–711.
[12] C. Chu, R. Li, F. Cai, Z. Bai, Y. Wang, X. Xu, N. Wang, J. Yang, S. Dou, *Energy Environ. Sci.* **2021**, *14*(8), 4318–4340.
[13] W. Luo, Y. Zhang, S. Xu, J. Dai, E. Hitz, Y. Li, C. Yang, C. Chen, B. Liu, L. Hu, *Nano Lett.* **2017**, *17*(6), 3792–3797.
[14] S. Wang, Y. Liu, K. Lu, W. Cai, Y. Jie, F. Huang, X. Li, R. Cao, S. Jiao, *Energy Fuels* **2021**, *35*(5), 4587–4595.
[15] Y. Cheng, Z. Wang, J. Chen, Y. Chen, X. Ke, D. Wu, Q. Zhang, Y. Zhu, X. Yang, M. Gu, *Angew. Chem.* **2023**, *135*(30), e202305723.
[16] J. L. Yang, X. X. Zhao, W. Zhang, K. Ren, X. X. Luo, J. M. Cao, S. H. Zheng, W. L. Li, X. L. Wu, *Angew. Chem.* **2023**, *135*(15), e202300258.
[17] J.-N. Chazalviel, *Physical review A* **1990**, *42*(12), 7355
[18] W. Zhang, C. D. Zhao, X. L. Wu, *Adv. Mater. Interfaces* **2020**, *7*(23), 2001444.
[19] Z. Shen, J. Huang, Y. Xie, D. Wei, J. Chen, Z. Shi, *ChemSusChem* **2024**, e202301777.
[20] K. Yu, J. Chen, X. Xie, K. Lin, J. Li, Z. Shi, *Surfaces* **2022**, *34*, 102326.
[21] R. Damircheli, B. Hoang, V. Castagna Ferrari, C.-F. Lin, *ACS Appl. Mater. Interfaces* **2023**, *15*(47), 54915–54922.
[22] Z. Hu, L. Liu, X. Wang, Q. Zheng, C. Han, W. Li, *Adv. Funct. Mater.* **2024**, *34*(22), 2313823.
[23] G. Wang, Y. Zhang, B. Guo, L. Tang, G. Xu, Y. Zhang, M. Wu, H.-K. Liu, S.-X. Dou, C. Wu, *Nano Lett.* **2020**, *20*(6), 4464–4471.
[24] Z.-Y. Gu, X.-T. Wang, Y.-L. Heng, K.-Y. Zhang, H.-J. Liang, J.-L. Yang, E. H. Ang, P.-F. Wang, Y. You, F. Du, *Science* **2023**, *S2095–9273*(2023), 00566–00562.
[25] P. Wróbel, P. Kubisiak, A. Eilmes, *J. Phys. Chem.* **2021**, *125*(4), 1248–1258.
[26] S. Wu, Y. Qiao, K. Jiang, Y. He, S. Guo, H. Zhou, *Adv. Funct. Mater.* **2018**, *28*(13), 1706374.
[27] J. Zhu, P. Li, X. Chen, D. Legut, Y. Fan, R. Zhang, Y. Lu, X. Cheng, Q. Zhang, *Energy Storage Mater.* **2019**, *16*, 426–433.
[28] J. Chen, T. Liu, M. Chu, K. Yu, X. Xie, K. Lin, Y. Cheng, X. Zhang, J. Li, Z. Shi, *J. Mater. Chem.* **2024**.
[29] M. Ma, Y. Lu, Z. Yan, J. Chen, *Batteries & Supercaps* **2019**, *2*(8), 663–667.
[30] Z. Xu, J. Yang, T. Zhang, L. Sun, Y. Nuli, J. Wang, S. I. Hirano, *Adv. Funct. Mater.* **2019**, *29*(27), 1901924.
[31] W. Liu, Z. Chen, Z. Zhang, P. Jiang, Y. Chen, E. Paek, Y. Wang, D. Mitlin, *Energy Environ. Sci.* **2021**, *14*(1), 382–395.
[32] D. Li, Y. Sun, M. Li, X. Cheng, Y. Yao, F. Huang, S. Jiao, M. Gu, X. Rui, Z. Ali, *ACS Nano* **2022**, *16*(10), 16966–16975.
[33] W. Luo, C.-F. Lin, O. Zhao, M. Noked, Y. Zhang, G. W. Rubloff, L. Hu, *Adv. Energy Mater.* **2017**, *7*(2), 1601526.
[34] S. Choudhury, Rational Design of Nanostructured Polymer Electrolytes and Solid-Liquid Interphases for Lithium Batteries[M]. Springer Nature, 2019.
[35] X. Gao, J. You, L. Deng, B. Zhang, Y. Li, W. Wang, *J. Mater. Chem.* **2024**.
[36] K.-Y. Zhang, Y.-Q. Fu, H.-H. Liu, J.-L. Yang, M.-Y. Su, Y. Wang, X.-L. Wu, *Physica Scripta J.* **2023**, *98*(12), 125977.
[37] E. Gabriel, C. Ma, K. Graff, A. Conrado, D. Hou, H. Xiong, *eScience.J.* **2023**, *3*(5), 100139.
[38] J. Chen, D. Li, K. Lin, X. Ke, Y. Cheng, Z. Shi, *J. Power Sources* **2022**, *540*, 231603.
[39] M. Xu, Y. Li, M. Ihsan-Ul-Haq, N. Mubarak, Z. Liu, J. Wu, Z. Luo, J. K. Kim, *Energy Storage Mater.* **2022**, *44*, 477–486.
[40] J. L. Ma, Y. B. Yin, T. Liu, X. B. Zhang, J. M. Yan, Q. Jiang, *Adv. Funct. Mater.* **2018**, *28*(13), 1703931.
[41] A. Petrongari, M. Tuccillo, A. Ciccioli, A. Latini, S. Brutti, *ChemElectroChem* **2023**, *10*(5), e202201074.
[42] M. Moorthy, B. Moorthy, B. K. Ganesan, A. Saha, S. Yu, D. H. Kim, S. Hong, S. Park, K. Kang, R. Thangavel, *Adv. Funct. Mater.* **2023**, *33*(42), 2300135.
[43] T. Deng, X. Ji, L. Zou, O. Chikeze, L. Cao, X. Fan, T. R. Adebisi, H.-J. Chang, H. Wang, B. Li, *Nat. Nanotechnol.* **2022**, *17*(3), 269–277.
[44] G. Wang, F. Yu, Y. Zhang, Y. Zhang, M. Zhu, G. Xu, M. Wu, H.-K. Liu, S.-X. Dou, C. Wu, *Nano Energy* **2021**, *79*, 105457.
[45] P. Viswanath, M. Yoshimura, *SN Appl. Sci.* **2019**, *1*(11), 1519.
[46] V. Nefedov, Y. A. Buslaev, Y. V. Kokunov, *Zh. Neorg. Khim.* **1974**, *19*(5), 1166–1169.
[47] C. Wagner, *Faraday Discuss.* **1975**, *60*, 291–300.
[48] D. Chadwick, T. Hashemi, *Corrosion* **1978**, *18*(1), 39–51.
[49] A. Barrie, F. Street, *J. Electron Spectrosc. Relat. Phenom.* **1975**, *7*(1), 1–31.
[50] H. Seyama, M. Soma, *J. Chem. Soc. Faraday Trans. 1* **1985**, *81*(2), 485–495.

Manuscript received: October 28, 2024

Revised manuscript received: November 27, 2024

Accepted manuscript online: December 23, 2024

Version of record online: January 7, 2025